

TESSERAQ: ULTRA LOW-BIT LLM POST-TRAINING QUANTIZATION WITH BLOCK RECONSTRUCTION

Anonymous authors

Paper under double-blind review

ABSTRACT

Large language models (LLMs) have revolutionized natural language processing, albeit at the cost of immense memory and computation requirements. Post-training quantization (PTQ) is becoming the *de facto* method to reduce the memory footprint and improve the inference throughput of LLMs. In this work, we aim to push the upper limit of LLM PTQ by optimizing the weight rounding parameters with the block reconstruction technique, a predominant method in previous vision models. We propose TesseraQ, a new state-of-the-art PTQ technique, to quantize the weights of LLMs to ultra-low bits. To effectively optimize the rounding in LLMs and stabilize the reconstruction process, we introduce progressive adaptive rounding. This approach iteratively transits the soft rounding variables to hard variables during the reconstruction process. Additionally, we optimize the dequantization scale parameters to fully leverage the block reconstruction technique. We demonstrate that TesseraQ can be seamlessly integrated with existing scaling or clipping-based PTQ algorithms such as AWQ and OmniQuant, significantly enhancing their performance and establishing a new state-of-the-art. For instance, when compared to AWQ, TesseraQ improves the wikitext2 perplexity from 14.65 to 6.82 and average downstream accuracy from 50.52 to 59.27 with 2-bit weight-only quantization of LLaMA-2-7B. Across a range of quantization schemes, including W2A16, W3A16, W3A3, and W4A4, TesseraQ consistently exhibits superior performance.

1 INTRODUCTION

Large Language Models (LLMs) have revolutionized natural language processing with their remarkable capabilities. LLMs such as, GPT-4 (Bubeck et al., 2023) and LLaMA-3 (Meta, 2024), contain hundreds of billions of parameters. While this scale enables their impressive performance, it also poses significant deployment challenges (Zhou et al., 2024). LLMs require substantial memory and computational resources, making them impractical for many real-world applications, especially on consumer devices or in resource-limited environments (Dettmers et al., 2022). Quantization addresses this issue by reducing the precision of the model’s parameters and activations, typically from 32-bit floating-point (FP32) to lower bit-width representations such as 8-bit or 4-bit integer (INT8, INT4). This technique significantly decreases the model’s memory footprint to increase the I/O throughput, often with marginal performance loss.

Post-Training Quantization (PTQ) (Gholami et al., 2022) has perhaps become the most widespread and the easiest way to compress the LLM by reducing the bitwidth of the pretrained model’s parameters. For example, with a single GPU and a small number of input sequences, GPTQ (Frantar et al., 2022) can compress an FP16 LLM into INT4 format by deriving the exact solution for quantization error minimization. Recent works like AWQ (Lin et al., 2023), QuaRot (Ashkboos et al., 2024) and OmniQuant (Shao et al., 2023) have pushed the compression limit further with INT3 weight-only quantization achieving a small performance gap with respect to the FP16 baseline. However, in a more challenging scenario like INT2 weight-only quantization and weight-and-activation quantization, these methods still incur a large performance gap compared to the original FP16 model.

We conjecture that the major reason for the low performance on ultra low-bit PTQ is limited optimization space. Most works only focus on optimizing distribution transformation or weight clipping ranges (Lin et al., 2023; Wei et al., 2023; Shao et al., 2023). While being straightforward, they prove inadequate for extremely low-bit scenarios due to the constrained optimization space. For instance,

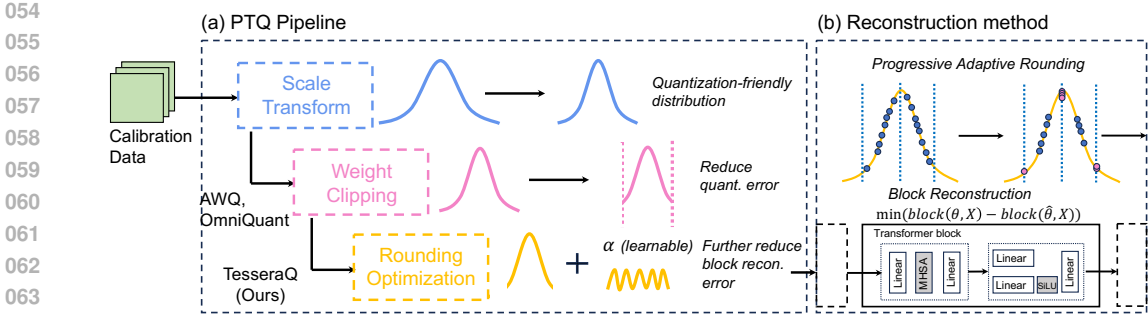


Figure 1: **The overall workflow of our proposed method.** (a) We apply TesseraQ to optimize the weight rounding parameters when the transformation scale and clipping range are determined using prior methods like AWQ/OmniQuant. (b) We propose Progressive Adaptive Rounding (PAR) for block-wise reconstruction, which iteratively hardens some rounding variables and optimizes the rest soft rounding variables till all variables become binary.

in per-channel weight quantization, a single clipping range or transformation scale must account for $4k \sim 20k$ weight elements in one channel, resulting in suboptimal quantization performance. We contend that to enhance LLM PTQ performance further, adjustment of the entire weight tensor is necessary. However, it is non-trivial to tune billions of parameters simultaneously.

To this end, we propose TesseraQ, a block reconstruction method tailored for LLM rounding optimization. We found that rounding optimization on a transformed and clipped LLM (Fig. 1(a)) brings significantly better performance than GPTQ. To accommodate the billions of parameter spaces in LLMs, our approach removes the dependency of regularization loss in the original rounding optimization processes (Nagel et al., 2020; Li et al., 2021) by introducing Progressive Adaptive Rounding (PAR). As shown in Fig. 1(b), PAR iteratively hard rounds certain rounding variables to binary values and optimizes the remainder to compensate for the rounding error. Moreover, we propose dequantization scale tuning to further decrease the reconstruction error. Leveraging block-wise reconstruction, we can efficiently and effectively optimize each LLM block on a single GPU. We have validated TesseraQ across various LLMs and uniform quantization bit-widths, demonstrating superior post-training performance and establishing new state-of-the-art quantized LLMs. We summarize our contributions as follows

1. We propose TesseraQ, a block reconstruction-based weight rounding optimization method for LLMs. TesseraQ can be combined with existing transformation or clipping methods like AWQ, OmniQuant, and QuaRot to obtain state-of-the-art results.
2. TesseraQ contains Progressive Adaptive Rounding and Dequantization Scale Tuning. Both methods can stabilize the reconstruction process and effectively optimize post-training performance.
3. Our method obtains state-of-the-art performance on both perplexity metric and zero-shot accuracy metric. For example, our method improves OmniQuant perplexity results from 37.4 to **8.0** on LLaMA-2-7B W2A16 quantization. Moreover, TesseraQ+QuaRot improves the average accuracy by **10%** on LLaMA-3.1-8B W3A3 quantization as compared to GPTQ+QuaRot.

2 PRELIMINARIES

This section briefly introduces the existing research directions in LLM PTQ. We adopt uniform affine quantization, which essentially discretizes the floating-point representation of weights/activations into low-bit fixed-point representation, given by

$$\mathbf{W}^q = \text{clamp}\left(\left\lfloor \frac{\mathbf{W}}{s} \right\rfloor + z, 0, 2^N - 1\right), \text{ where } s = \frac{\gamma \max(\mathbf{W}) - \beta \min(\mathbf{W})}{2^N - 1}, z = -\left\lfloor \frac{\beta \min(\mathbf{W})}{s} \right\rfloor. \quad (1)$$

where s and z denote the quantization step size and the zero point. The resulting \mathbf{W}^q is in the INT- N format. To restore it back to its original range, the dequantization step is given by $\hat{\mathbf{W}} = s \times (\mathbf{W}^q - z)$.

Optimization Objective. The plain rounding-to-nearest (RTN) method directly quantifies the model weights to integers without further optimization. However, this method usually results in

significantly low task performance. To improve the LLM PTQ performance, parameters related to quantization are optimized with different objectives. For example, GPTQ (Frantar et al., 2022) and AWQ (Lin et al., 2023) utilize the layer-wise reconstruction objective, given by

$$\min_{\epsilon} (\mathbf{L}(\theta + \epsilon) - \mathbf{L}(\theta)) \approx \sum_{\ell=1}^L \|\hat{\mathbf{W}}^{(\ell)} \mathbf{X}^{(\ell)} - \mathbf{W}^{(\ell)} \mathbf{X}^{(\ell)}\|_F^2, \quad (2)$$

where \mathbf{L} is the loss function parameterized by weights in the whole model θ and quantization noise $\epsilon = \hat{\theta} - \theta$. $\ell \in \{1, 2, \dots, L\}$ is the layer index and \mathbf{X} is the input activations. While this layer-wise objective can provide efficient and exact solutions as in GPTQ, the objective does not consider inter-layer correlation like self-attention and residual connections in LLM. To this end, the block-wise reconstruction objective has been proposed (Li et al., 2021), as

$$\min_{\epsilon} (\mathbf{L}(\theta + \epsilon) - \mathbf{L}(\theta)) \approx \sum_{b=1}^B \|\text{block}(\hat{\theta}^{(b)}, \mathbf{X}^{(b)}) - \text{block}(\theta^{(b)}, \mathbf{X}^{(b)})\|_F^2. \quad (3)$$

where, block refers to one decoder block in LLMs comprising self-attention, projection, feed-forward and normalization layers. In practice, both layer-wise and block-wise objectives enable efficient calibration on a single GPU due to their local computation attributes. However, block-wise objectives exhibit better performance than layer-wise objectives as they better approximate the global loss (i.e., Eq. (3) left side) by accounting for contributions from multiple layers.

Optimization Space. Generally, three kinds of optimization spaces are explored in LLM PTQ, (1) the scale transformation, (2) the clipping range (i.e., finding the suitable γ, β), and (3) the weight values. They can be tied with either layer-wise or block-wise objectives. For instance, AWQ (Lin et al., 2023) and OS+ (Wei et al., 2023) optimize transformation and clipping range using Eq. (2), while OmniQuant (Shao et al., 2023) does similar optimization with Eq. (3). Since scale/clipping optimization methods are well-explored, in this paper, we aim to optimize weight values using block-wise objectives to further push the compression limits of LLM PTQ.

3 TESSERAQ: ULTRA LOW-BIT POST-TRAINING QUANTIZATION

3.1 PROBLEM STATEMENT

Element-wise weight adjustments were also studied in GPTQ (Frantar et al., 2022), in which the weights are computed using closed-form solutions using the inverse Hessian matrix. However, this technique makes it hard to improve scale-transformed models like AWQ¹. Gong et al. (2024) also report similar observations with GPTQ. We hypothesize that the reason for the failed improvement of GPTQ+AWQ could be the layer-wise reconstruction objective and its approximation for the Hessian matrix, for example, to compute the inverse Hessian they dampen the matrix by $\lambda \mathbf{I}$.

In this work, we select a different weight optimization framework, the rounding optimization (Nagel et al., 2020; Li et al., 2021), which is a different optimization space compared to GPTQ, given by

$$\begin{aligned} \min_{\alpha} \quad & \|\text{block}(\hat{\theta}, \mathbf{X}) - \text{block}(\theta, \mathbf{X})\|_F^2, \\ \text{s.t.} \quad & \hat{\theta} = \mathbf{s} \times (\theta^q - \mathbf{z}), \quad \theta^q = \text{clamp}\left(\left\lfloor \frac{\theta}{\mathbf{s}} \right\rfloor + \alpha + \mathbf{z}, 0, 2^N - 1\right), \quad \alpha \in \{0, 1\}^d. \end{aligned} \quad (4)$$

Here, θ denotes the total d weight parameters of linear layers in the block, α is the rounding variable. Note that we omit the block index for simplicity. This rounding optimization framework shares both pros and cons. For its pros, rounding optimization space restricts the range of each weight parameter, allowing us to further improve the other PTQ models like AWQ/OmniQuant/QuaRot by slightly adjusting each weight element. As for its cons, there is no closed-form solution for rounding variables under the block-reconstruction framework. In addition, the binary rounding variables require either continuous relaxation with regularization loss (Nagel et al., 2020) or Straight-Through Estimator (Hubara et al., 2020) to be optimized. Thus, optimizing billions of rounding variables is challenging (Frantar et al., 2022). In Appendix A, we also show traditional rounding optimization is hard to scale on LLMs.

¹GPTQ can be combined with rotation-transformed models like QuaRot. We also compare it in Sec. 4.

Algorithm 1: TesseraQ Calibration process

Input: FP16 LLM model; Calibration dataset, PAR iteration K , training steps T

for all $b = 1, 2, \dots, B$ -th block in the FP model **do**

 Collect input data to the block \mathbf{X} , the FP output $\text{block}(\theta, \mathbf{X})$;

 Initialize rounding variable ν , dequantization scale \mathbf{v} ;

for all $k = 1, 2, \dots, K$ -iteration **do**

 Calculate score (Eq. (6)) and hard-round the variables with lowest $P_k\%$ scores;

for all $t = 1, 2, \dots, T$ -training steps **do**

 Gradient Descend Eq. (7) and update the soft rounding variables in this block as well as the dequantization scale;

 Set all rounding variables to 0/1 and merge them into original parameters;

return Quantized model;

3.2 PROGRESSIVE ADAPTIVE ROUNDING

To optimize α , we introduce a differentiable rounding optimization framework called progressive adaptive rounding (PAR) that does not rely on regularization loss or the straight-through estimator in contrast to previous works (Nagel et al., 2020; Hubara et al., 2020).

To start with, we relax the rounding variable into a continuous variable by using the Sigmoid reparameterization $\alpha = \sigma(\nu)$. Therefore, ν can be initialized as $\nu = \sigma^{-1}(\theta/s - \lfloor \theta/s \rfloor)$, resulting in $\hat{\theta} = \theta$. The PAR algorithm divides all rounding variables into two sets: $\mathcal{S}_{\text{Hard}}$ and $\mathcal{S}_{\text{Soft}}$, standing for the *hard* and *soft* rounding of the variable ν . Formally, we define the rounding function as

$$\alpha_i = \begin{cases} \sigma(\nu_i) = \frac{1}{1+\exp(-\nu)} & \text{if } i \in \mathcal{S}_{\text{Soft}} \\ \sigma'(\nu_i) = \mathbf{1}_{\nu_i > 0} & \text{if } i \in \mathcal{S}_{\text{Hard}} \end{cases}. \quad (5)$$

The $\sigma'(\nu_i)$ is a hard rounding function that returns 1 if ν_i is larger than 0, otherwise it returns 0. Starting from an empty hard rounding set, we iteratively put variables from $\mathcal{S}_{\text{Soft}}$ into $\mathcal{S}_{\text{Hard}}$ (called *Harden Phase*), and optimize the remaining soft rounding variables to compensate for the hard rounding loss (called *Soften Phase*). We elaborate on them in the following two subsections.

Harden Phase. Intuitively, after setting rounding variables to hard ones, we would expect minimum loss change in the block output error. Therefore, we define a score metric

$$HS(\nu) = |\sigma(\nu) - 0.5|. \quad (6)$$

Essentially, the lower the score, the closer the soft rounding variable ($\sigma(\nu)$) is to 0.5, implying that rounding these variables to binary values will result in a larger increase in reconstruction loss. As a result, in the Harden Phase, we sort the parameter indices based on their HS and select the lowest $P\%$ of them to $\mathcal{S}_{\text{Hard}}$. The hyper-parameter P should increase from 0 to near 100 during block reconstruction. During the early stage of the reconstruction, P can be increased rapidly, however, in the later stage, we slowly increase P since the learnable soft variables are becoming fewer in each iteration. In our experiments, we find that TesseraQ is not sensitive to any specific decay schedule for P , as long as we progressively slow down the increasing rate of P . We conduct an ablation study of how to schedule the change of P in Sec. 4.3.

Soften Phase. For this stage, we employ the gradient-descent optimization to optimize the soft rounding variable

$$\min_{\nu_i, i \in \mathcal{S}_{\text{Soft}}} \|\text{block}(\hat{\theta}, \mathbf{X}) - \text{block}(\theta, \mathbf{X})\|_F^2. \quad (7)$$

This objective can be optimized via gradient-based training like Adam (Kingma, 2014). During implementation, it would be too expensive to use masking to indicate soft rounding or hard rounding. Instead, for memory-efficient implementation, we can safely set the hard-rounding variables to ∞ or $-\infty$, which returns zero gradients in the sigmoid function. We find that optimizing Eq. (7) with nearly 200 steps can sufficiently decrease the block reconstruction error across different LLM models.

Post-Processing. After the entire PAR procedure is finished, we apply hard-rounding $\sigma'(\cdot)$ to all variables merge their values into the original weights, and then we can use the standard quantization formula (i.e., Eq. (1)). The merging can be effectively implemented by

$$\theta \leftarrow \theta + \mathbf{s} \times (\sigma'(\nu) - 0.5) \quad (8)$$

We provide a pseudocode for the learning process in Algorithm 1.

3.3 DEQUANTIZATION SCALE TUNING

During the PAR process, the quantized tensor θ^q undergoes continuous changes. To accommodate these dynamic adjustments, we propose a method that optimizes the dequantization scale concurrently with the rounding variable. Specifically, for the dequantization step, we introduce an additional parameter \mathbf{v} and represent it as

$$\hat{\theta} = 2\sigma(\mathbf{v}) \times \mathbf{s} \times (\theta^q - \mathbf{z}). \quad (9)$$

By initializing $\mathbf{v} = \mathbf{0}$, we initialize the dequantization scale factor ($2\sigma(\mathbf{v})$) to 1 and subsequently adjust it to a value within the range (0, 2). The sigmoid reparameterization can smooth the training process and reduce the efforts to adjust learning rate hyper-parameter. Note that we avoid optimizing the scale s in the quantization step (Eq. (1)) since, (1) any change in s would result in a change of the rounding mechanism (Nagel et al., 2020), (2) the optimization requires straight-through estimation (Shao et al., 2023) which leads to biased gradient calculation. Experiments in Sec. 4.3 demonstrate that dequantization scale tuning can benefit the final quantization performance of TesseraQ by a large margin.

4 EXPERIMENTS

4.1 EXPERIEMENTS SETUP

Most of our experiment setups are similar to OmniQuant (Shao et al., 2023), which also adopts block reconstruction loss function. Specifically, we employ asymmetric uniform quantization with 2/3/4-bit integers. We test both per-group and per-channel weight quantization. For example, we use the notation *W2A16g64* to denote the 2-bit per-group (group size is set to 64) weight-only quantization, where activations are FP16. In weight-activation quantization experiments (all INT precision), defaults are W4A4, W3A3, and W4A8 with per-channel weight and per-token activation quantization (Dettmers et al., 2022; Shao et al., 2023).

Calibration Data and Comparison. We report two types of evaluation metrics, the perplexity metric for evaluating the upstream datasets like WikiText2 (Merity et al., 2016), C4 (Raffel et al., 2020), and the average accuracy of 5 downstream reasoning tasks including PIQA (Bisk et al., 2020), ARC easy/challenge (Clark et al., 2018), WinoGrande (Sakaguchi et al., 2021) and HellaSwag (Zellers et al., 2019). The perplexity is evaluated with 2048 sequences. We use 512 2048-token segments from the WikiText2 training dataset as calibration data for perplexity comparison and for downstream task comparison, we sample same amount of calibration data from the C4 training dataset. We use `lm_eval` (ver0.4.2) to evaluate the accuracy.

Training. We set the total PAR number of iterations K to 20 and gradually increase the P_k from 0 to 100%. In each iteration, we optimize the learnable parameters (ν and \mathbf{v}) for 250 training steps. We use the Adam optimizer with a fixed learning rate of $1e - 3$. We add $1e - 4$ weight decay to \mathbf{v} during training. The batch size is set to 4. We use AWQ transformation (Lin et al., 2023) to initialize our model since we find AWQ initialization is slightly better than OmniQuant across all configurations except W2A16 quantization. For W2A16, AWQ yields very high perplexity. Thus, in the W2A16 case, we directly use the pretrained OmniQuant model for initialization.

Models and Baselines. For the upstream tasks, we follow OmniQuant (Shao et al., 2023) to test weight-only quantization results on LLaMA-1-7B/13B/30B/65B (Touvron et al., 2023a), LLaMA-2-7B/13B/70B (Touvron et al., 2023b) and LLaMA-3-8B/70B (Meta, 2024). In this case, we compare GPTQ (Frantar et al., 2022), OmniQuant (Shao et al., 2023), AWQ (Lin et al., 2023), SignRound (Cheng et al., 2023) and GPTQ with QuaRot Ashkboos et al. (2024). For downstream tasks, we test LLaMA-2-7B, LLaMA-3.1-8B/70B across 5 downstream tasks. We compare GPTQ, AWQ, OmniQuant, and SignRound.

Table 1: **Weight-only quantization results of LLaMA-1/2/3 models.** We report WikiText2 perplexity (PPL \downarrow). *, †, ‡ means initialized from AWQ, OmniQuant, and QuaRot, respectively.

| LLaMA1&2 | Method | 1-7B | 1-13B | 1-30B | 1-65B | 2-7B | 2-13B | 2-70B | 3-8B | 3-70B |
|-----------------------------|-----------------------------|-------------|-------------|-------------|-------------|-------------|-------------|--------------|--------------------------|--------------------------|
| FP16 | - | 5.68 | 5.09 | 4.10 | 3.53 | 5.47 | 4.88 | 3.31 | 6.14 | 2.85 |
| W2A16 | GPTQ | 2.1e3 | 5.5e3 | 499.75 | 55.91 | 7.7e3 | 2.1e3 | 77.95 | 8.4e4 | 1.6e4 |
| | GPTQ [‡] | 11.13 | 9.14 | 7.04 | 5.91 | 18.77 | 10.84 | 5.68 | 24.98 | 16.29 |
| | AWQ | 1.1e5 | 7002 | 1.2e5 | 6.3e6 | 2.9e6 | 6.2e3 | 3973 | 4.1e5 | 8.6e4 |
| | OmniQuant | 15.47 | 13.21 | 8.71 | 7.58 | 37.37 | 17.21 | 7.81 | - | - |
| | TesseraQ[†] | 7.56 | 6.56 | 5.75 | 5.21 | 8.05 | 6.55 | 5.26 | 17.88[‡] | 11.56[‡] |
| W2A16 g128 | GPTQ | 44.01 | 15.60 | 10.92 | 9.51 | 36.77 | 28.14 | NAN | 226.7 | 16.06 |
| | GPTQ [‡] | 16.25 | 8.14 | 6.62 | 5.61 | 16.10 | 9.29 | 5.32 | 17.43 | 30.89 |
| | AWQ | 13.08 | 10.02 | 7.46 | 6.08 | 14.65 | 8.93 | 5.72 | 334.1 | 10.98 |
| | SignRound | 641.8 | 8.36 | 7.13 | 5.52 | NAN | 7.64 | NAN | - | - |
| | OmniQuant | 9.72 | 7.93 | 7.12 | 5.95 | 11.06 | 8.26 | 6.55 | - | - |
| TesseraQ[*] | 6.92 | 6.07 | 5.26 | 4.83 | 6.82 | 5.92 | 4.73 | 10.03 | 7.47 | |
| W2A16 g64 | GPTQ | 22.10 | 10.06 | 8.54 | 8.31 | 20.85 | 22.44 | NAN | 86.32 | 11.78 |
| | GPTQ [‡] | 11.44 | 7.70 | 6.23 | 5.26 | 15.30 | 9.17 | 5.19 | 16.58 | 21.50 |
| | AWQ | 10.65 | 8.66 | 6.65 | 5.58 | 11.87 | 7.81 | 5.30 | 53.07 | 9.04 |
| | OmniQuant | 8.90 | 7.34 | 6.59 | 5.65 | 9.62 | 7.56 | 6.11 | - | - |
| | TesseraQ[*] | 6.78 | 5.97 | 5.18 | 4.70 | 6.67 | 5.81 | 4.60 | 9.28 | 6.96 |
| W3A16 | GPTQ | 8.06 | 6.76 | 5.84 | 5.06 | 8.37 | 6.44 | 4.82 | 16.84 | 18.94 |
| | GPTQ [‡] | 6.15 | 5.45 | 4.53 | 4.01 | 6.13 | 5.35 | 3.72 | 7.54 | 5.22 |
| | AWQ | 8.49 | 6.38 | 5.89 | 6.03 | 14.17 | 6.42 | 4.22 | 11.79 | 12.28 |
| | OmniQuant | 6.49 | 5.68 | 4.74 | 4.04 | 6.58 | 5.58 | 3.92 | - | - |
| | TesseraQ[*] | 5.99 | 5.35 | 4.44 | 3.89 | 5.84 | 5.16 | 3.68 | 7.46 | 5.12 |
| W3A16 g128 | GPTQ | 6.55 | 5.62 | 4.80 | 4.17 | 6.29 | 5.42 | 3.85 | 9.58 | 5.25 |
| | GPTQ [‡] | 6.07 | 5.41 | 4.48 | 3.92 | 5.99 | 5.28 | 3.65 | 7.42 | 4.98 |
| | AWQ | 6.38 | 5.52 | 4.59 | 3.92 | 6.19 | 5.30 | 3.72 | 8.24 | 4.63 |
| | SignRound | 6.28 | 5.45 | 4.50 | 3.90 | 8.09 | 5.23 | 3.68 | - | - |
| | OmniQuant | 6.15 | 5.44 | 4.56 | 3.94 | 6.03 | 5.28 | 3.78 | - | - |
| TesseraQ[*] | 5.95 | 5.32 | 4.40 | 3.82 | 5.71 | 5.11 | 3.61 | 6.90 | 4.13 | |
| W4A16 | GPTQ | 6.13 | 5.40 | 4.48 | 3.83 | 5.83 | 5.13 | 3.58 | 7.28 | 4.94 |
| | GPTQ [‡] | 5.78 | 5.20 | 4.24 | 3.65 | 5.61 | 5.00 | 3.42 | 6.57 | 3.59 |
| | AWQ | 5.99 | 5.24 | 4.30 | 3.71 | 5.82 | 5.07 | 3.49 | 7.09 | 5.19 |
| | OmniQuant | 5.86 | 5.21 | 4.25 | 3.71 | 5.74 | 5.02 | 3.47 | - | - |
| | SignRound | 5.93 | 5.21 | 4.23 | 3.65 | 5.81 | 5.00 | 3.40 | - | - |
| TesseraQ[*] | 5.78 | 5.17 | 4.20 | 3.63 | 5.56 | 4.96 | 3.40 | 6.48 | 3.33 | |

4.2 MAIN RESULTS

Perplexity Evaluation. We summarized the Wikitext2 perplexity (PPL) results in Table 1. Our method consistently outperforms existing methods like AWQ and OmniQuant, particularly for the low-bit W2A16 configuration. Remarkably, in the W2A16 case, all existing methods except OmniQuant and GPTQ with QuaRot failed to successfully quantize the models (yielding $> 1e3$ perplexity). On the LLaMA-2-7B model, OmniQuant only obtains 37.37 PPL while our method largely improves this result to **8.05**. In addition, LLaMA-3-8B demonstrates extremely low quantization resiliency, where the AWQ model crashed in W2A16g128 quantization. Our method, on the other hand, significantly improves the wikitext2 PPL from 334 to 10.03. We observe that in general, the lower the bitwidth, the more improvement we can obtain from TesseraQ. This confirms our initial intuition that extremely low-bit weight quantization requires a thorough adjustment of each weight element. Additionally, the C4 (Raffel et al., 2020) PPL results are provided in Appendix: Table 9. Note that the C4 results for OmniQuant are re-evaluated from the official checkpoint to align the evaluation protocol. Overall, C4 PPL results concur with the Wikitext2 results, demonstrating a similar trend in performance improvement. For example, TesseraQ improves the PPL of LLaMA-2-7B model from 90.64 to 14.82 with W2A16 quantization.

Downstream Tasks Evaluation. We also test the weight-only quantization performance on five reasoning tasks. The results are summarized in Table 2, for LLaMA-2-7B, LLaMA-3.1-8B/70B². Notably, we found that the LLaMA-3.1-8B model demonstrates low quantization resiliency, as also shown in Huang et al. (2024c). For example, with W2A16g128 AWQ, this model drops more than 30% average accuracy on downstream tasks, while the gap is 15% for the LLaMA-2-7B model. Fortunately, our TesseraQ can substantially increase the average performance on the downstream

²We did not implement OmniQuant on LLaMA-3.1 models due to its high resource & time demands.

Table 2: **Weight-only quantization Results of various LLMs.** We report the accuracy of 5 common sense reasoning tasks (\uparrow). * means initialized from AWQ.

| Models | Bitwidths | Methods | PiQA | ArcE | ArcC | HellaSwag | WinoGrande | Avg. | |
|------------------|------------------|------------------|--------------|--------------|--------------|--------------|--------------|--------------|-------|
| LLaMA-2-7B | FP16 | - | 78.07 | 76.34 | 43.51 | 57.17 | 69.21 | 64.87 | |
| | | GPTQ | 58.21 | 33.75 | 19.79 | 29.60 | 51.30 | 38.53 | |
| | W2A16 g128 | AWQ | 67.73 | 55.47 | 28.74 | 41.37 | 59.27 | 50.52 | |
| | | OmniQuant | 64.79 | 51.13 | 24.83 | 40.30 | 56.90 | 47.59 | |
| | | SignRound | 72.96 | 65.99 | 32.25 | 47.35 | 61.01 | 55.92 | |
| | | TesseraQ* | 75.13 | 70.03 | 35.83 | 50.17 | 65.19 | 59.27 | |
| | W3A16 g128 | GPTQ | 76.65 | 73.69 | 40.52 | 54.43 | 66.61 | 52.39 | |
| | | AWQ | 76.71 | 73.56 | 41.63 | 54.79 | 67.64 | 62.87 | |
| | | OmniQuant | 76.93 | 74.66 | 39.59 | 54.95 | 67.16 | 62.66 | |
| | | SignRound | 76.82 | 75.25 | 42.92 | 55.33 | 68.27 | 63.72 | |
| TesseraQ* | 77.58 | 74.45 | 41.46 | 55.47 | 68.90 | 63.59 | | | |
| LLaMA-3.1-8B | FP16 | - | 80.08 | 81.43 | 51.19 | 59.95 | 73.55 | 69.25 | |
| | | GPTQ | 53.86 | 26.55 | 20.64 | 27.87 | 53.35 | 36.46 | |
| | W2A16 g128 | AWQ | 57.34 | 35.18 | 18.26 | 28.05 | 53.27 | 38.42 | |
| | | TesseraQ* | 75.68 | 68.98 | 35.66 | 50.21 | 66.29 | 59.37 | |
| | W3A16 g128 | GPTQ | 77.53 | 75.04 | 43.60 | 56.15 | 71.66 | 64.80 | |
| | | AWQ | 77.91 | 77.77 | 44.62 | 54.89 | 70.56 | 65.15 | |
| | TesseraQ* | 79.27 | 79.46 | 47.35 | 57.80 | 72.93 | 67.36 | | |
| | LLaMA-3.1-70B | FP16 | - | 83.13 | 87.12 | 60.92 | 66.47 | 79.56 | 75.44 |
| | | | GPTQ | 65.83 | 49.54 | 26.19 | 42.74 | 61.33 | 49.11 |
| | | W2A16 g128 | AWQ | 73.45 | 68.01 | 40.27 | 48.11 | 62.19 | 58.40 |
| TesseraQ* | | | 78.23 | 78.70 | 47.35 | 57.91 | 71.74 | 66.79 | |
| W3A16 g128 | | GPTQ | 80.79 | 82.70 | 55.54 | 63.18 | 77.03 | 71.85 | |
| | | AWQ | 81.72 | 84.89 | 55.98 | 63.71 | 78.68 | 72.99 | |
| TesseraQ* | | 82.86 | 85.52 | 58.70 | 64.99 | 78.37 | 74.09 | | |

tasks, bringing the gap between W2 and FP16 to only 9%. TesseraQ also outperforms a recent rounding optimization method, SignRound (Cheng et al., 2023), for W2A16g128, demonstrating the effectiveness of our method.

Weight-Activation Quantization Evaluation. Finally, we test weight-activation quantization scenarios with per-channel weight quantization and per-token activation quantization. With quantized activations, the inference speed of LLMs on GPUs/TPUs can be improved especially in the prefill stage (Lin et al., 2023). We experiment with W4A4, and W4A8 quantization and compare with three baselines, SmoothQuant, OS+, AWQ, QLLM (Liu et al., 2023a). The results are provided in Table 3. Table 3 summarizes the perplexity on WikiTex2, C4 and average accuracy on downstream tasks. (The detailed accuracy of each downstream task is located in Appendix: Table 13.) We observe a consistent improvement of 7% accuracy with TesseraQ compared to AWQ. Additionally, we also combine our method with a recent rotation-based quantization method, QuaRot (Ashkboos et al., 2024), and compare QuaRot+GPTQ and QuaRot+TesseraQ with W4A4 and W3A3 quantization. Combined with QuaRot, TesseraQ also exceeds GPTQ by 10% accuracy on the 8B model with W3A3 quantization, demonstrating the superiority of TesseraQ.

Results on Mistral-7B. Additionally, we also test the performance of our method on the Mistral-7B model Jiang et al. (2023), which achieves high pretrained accuracy and demonstrates higher quantization resiliency. We test its weight-only quantization (W2A16g128, W3A16g128) and weight-activation quantization (W4A4, W4A8) performance in the Appendix (Table 12). Our TesseraQ consistently outperforms other methods like SignRound, AWQ, and GPTQ.

4.3 ABLATION STUDIES

Below ablation studies are conducted with the LLaMA-2-7B model with W2A16g128 quantization.

Calibration Data. In this section, we compare the performance of different calibration datasets and sizes. We sample calibration data from either WikiText2 (Merity et al., 2016) or C4 (Raffel et al., 2020) training dataset. We also experiment with the different sample sizes, ranging from 128 to 512. Meanwhile, we change the batch size during rounding optimization, ranging from 1 to 4.

Table 3: **W4A4/W3A3 quantization results of LLaMA-1/2/3**. We use per-channel weight quantization and per-token activation quantization *, † means initialized from AWQ, QuaRot.

| Bitwidths | Methods | LLaMA-7B | | | LLaMA-2-7B | | | LLaMA-3.1-8B | | |
|-----------|------------------|--------------|--------------|--------------|--------------|--------------|--------------|--------------|--------------|--------------|
| | | WT2(↓) | C4(↓) | Avg. (↑) | WT2(↓) | C4(↓) | Avg. (↑) | WT2(↓) | C4(↓) | Avg. (↑) |
| FP16 | Pretrained | 5.68 | 7.08 | 62.30 | 5.47 | 6.97 | 64.87 | 6.24 | 9.54 | 69.25 |
| W4A4 | SmoothQuant | 585.1 | 780.5 | 37.02 | NAN | NAN | 35.29 | 654.6 | 508.5 | 36.09 |
| | OS+ | 16.47 | 25.51 | 50.50 | 29.03 | 39.71 | 50.50 | 124.2 | 67.44 | 40.71 |
| | AWQ | 12.67 | 17.58 | 48.41 | 13.87 | 19.54 | 49.99 | 60.99 | 74.08 | 42.51 |
| | OmniQuant | 11.26 | 14.51 | 50.47 | 14.61 | 18.39 | 49.86 | - | - | - |
| | QLLM | 9.65 | 12.29 | 51.84 | 11.75 | 13.26 | 51.60 | - | - | - |
| | TesseraQ* | 8.90 | 12.29 | 55.45 | 9.18 | 12.55 | 55.12 | 25.73 | 30.71 | 50.87 |
| | Atom (W4A4g128) | 6.16 | 7.70 | 60.17 | 6.14 | - | - | - | - | - |
| | QuaRot | 8.37 | 11.44 | 55.38 | 14.19 | 19.72 | 47.57 | 17.83 | 28.08 | 51.83 |
| W3A3 | GPTQ† | 6.16 | 8.37 | 61.37 | 6.16 | 8.44 | 61.45 | 8.39 | 13.24 | 62.87 |
| | TesseraQ† | 6.27 | 8.07 | 61.92 | 6.23 | 8.23 | 61.75 | 8.05 | 12.62 | 65.12 |
| | Atom (W3A3g128) | 11.77 | 15.43 | 49.28 | - | - | - | - | - | - |
| W3A3 | QuaRot | 2315 | 1665 | 35.53 | 10996 | 10940 | 35.18 | 91551 | 65662 | 35.25 |
| | GPTQ† | 11.57 | 13.89 | 50.82 | 14.54 | 20.76 | 44.62 | 93.08 | 104.73 | 37.87 |
| | TesseraQ† | 10.79 | 13.68 | 51.10 | 13.90 | 15.08 | 50.13 | 27.80 | 30.81 | 47.33 |

Table 4: **Ablation studies of calibration data source and data sizes**. We report the LLaMA-2-7B W2A16g128 quantization results with task performances and calibration costs.

| #Samples | BS | Runtime/ GPU Mem. | Calib. Data: WikiText2 | | | Calib. Data: C4 | | |
|----------|----|----------------------|------------------------|-------|---------|-----------------|--------------|--------------|
| | | | WikiText2(↓) | C4(↓) | Avg.(↑) | WikiText2(↓) | C4(↓) | Avg.(↑) |
| 128 | 1 | 3.2h/17.5GB | 7.33 | 11.39 | 56.58 | 8.54 | 10.83 | 56.87 |
| 256 | 2 | 3.9h/28.6GB | 7.10 | 11.16 | 57.17 | 8.32 | 10.66 | 57.85 |
| 512 | 2 | 4.0h/40.4GB | 7.14 | 11.22 | 57.42 | 8.22 | 10.47 | 58.56 |
| 512 | 4 | 6.0h/65.4GB | 6.82 | 10.77 | 58.35 | 8.05 | 10.29 | 59.27 |

Table 4 demonstrates the task performance (PPL and average accuracy metric) as well as the calibration costs (algorithm runtime and GPU memory footprint). First, we find that the source of calibration data will impact the perplexity evaluation. The performance benefits if evaluation data and calibration data are from the same dataset. For example, the C4-calibrated model has 1.2 higher WikiText2 PPL than the WikiText2-calibrated model. Second, increasing the number of samples and the batch size consistently improves the task performance. However, it may also lead to higher runtime and GPU memory consumption, which may be alleviated via multi-GPU calibration. Nevertheless, it is worthwhile to note that even with 128 samples and a batch size of 1, our TesseraQ can significantly improve the baseline AWQ results.

Algorithm choices. We also test the algorithm choices in TesseraQ. To be more specific, we experiment with block reconstruction with or without progressive adaptive rounding (PAR) and dequantization scale tuning (DST) and compare their final task performance. As shown in Table 5, both PAR and DST contribute a lot to the final perplexity metric (denoted by WT2 (WikiText2) and C4) and average accuracy (denoted by Avg.). Remarkably, applying one of them solely can also improve the AWQ baseline (first row) results by a large margin.

Table 5: TesseraQ Algorithm choices.

| PAR | DST | WT2 | C4 | Avg. |
|-----|-----|-------------|--------------|--------------|
| ✗ | ✗ | 14.65 | 18.67 | 50.52 |
| ✓ | ✗ | 7.72 | 11.95 | 56.79 |
| ✗ | ✓ | 8.58 | 13.14 | 54.45 |
| ✓ | ✓ | 6.82 | 10.77 | 58.35 |

PAR Schedule. We investigate how to adjust the P during progressive adaptive rounding. In our implementation, we use a handcrafted design, which manually decreases the soft rate (i.e., the percentage of soft rounding variable) as shown in Fig. 2. Our handcrafted design gradually decays the soft rate. To demonstrate that our PAR is quite robust to the schedule of soft rate, we also test several rule-based adjustments, which adjust the soft rate as $\frac{1}{\exp(tx)}$, where $x \in (0, 1]$ is the scaled iteration number and t is the temperature hyper-parameter. We test $t = \{2, 3, 4, 5, 6, 7\}$ and compare it with our handcrafted implementation with LLaMA-2-7B W2A16g128 quantization. The results in Fig. 2 show that $t = 4, 5$ and our handcrafted adjustments obtain the best performance. Overall, we find that our algorithm is not sensitive to the scheduling, and has consistently superior performance than the AWQ initialized model.

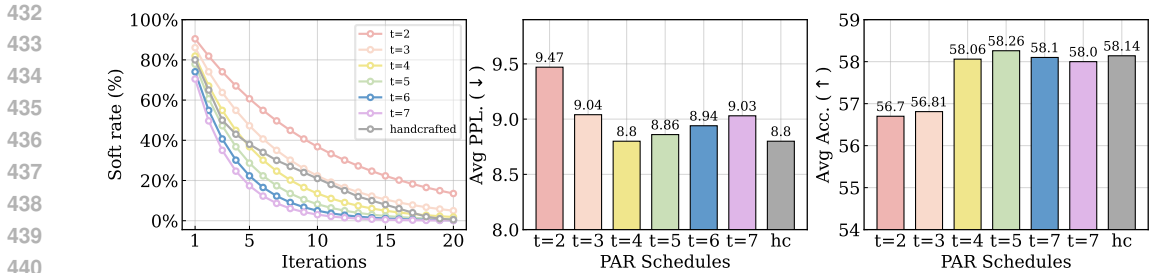


Figure 2: **Ablation study of PAR schedule.** We experiment several rule-based P adjustments and one handcrafted adjustment. (AWQ baseline results: average PPL: 16.66, average acc.: 50.52).

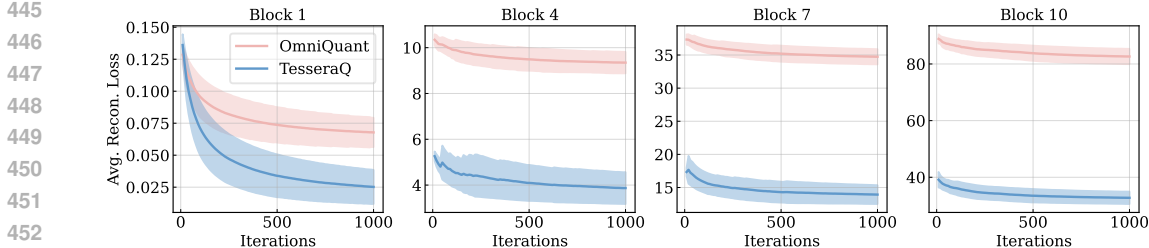


Figure 3: **Reconstruction loss convergence.** We compare the block reconstruction loss of OmniQuant and TesseraQ during optimization. Our method significantly reduces the loss in each block.

4.4 VISUALIZATION

In this section, we provide visualizations of our calibration process to interpret the effectiveness of our method. The experiments are conducted on LLaMA-2-7B with W2A16g128 quantization. We first compare the loss convergence value in OmniQuant and TesseraQ, both of which calibrate the model with block reconstruction loss. To ensure a fair comparison, we use the same AWQ initialization to these two methods and align all training hyper-parameters. As shown in Fig. 3, during the first block reconstruction, TesseraQ reduces more loss than OmniQuant. In the following blocks, the loss gap between our method and OmniQuant keeps on increasing. Consequently, TesseraQ will have a much lower model output error due to the cumulative effect of reconstruction.

Since rounding variables (α) are binary, we also demonstrate the number or percentage of rounding variables that flip after TesseraQ. In Table 6, we show the number and the percentage of flipped variables. Overall we observe around 3%~8% of variables flip, amounting to over 10M parameters per block. This proves that tensor-wise adjustment can be used to significantly improve previous scale transformation adjustments like AWQ. We also found that attention layers tend to have less flipped rounding compared to MLP layers. 2/3-bit quantization also flips more than 4-bit quantization.

4.5 HARDWARE EVALUATION

To demonstrate the weight compression effect and the inference throughput change, we test LLaMA-3.1-8B/70B/405B under different GPU environments, kernel backend and different bitwidths. Table 7 summarizes the results of inference throughput (generated token per second) with batch size 1 or 16. Remarkably, W2A16g128 reduces the weight memory of the 405B model from 756GB to 114 GB and the 70B model from 132 GB to 21 GB. However, the INT2 dequantization kernel (in Triton (JonathanSalwan) support) is currently less optimized, especially for larger models, expending lower throughput compared to FP16. We find that INT4 with Exllama kernel can increase the throughput when batch size is 1 and achieve similar throughput with FP16 model when batch size is 16. Nonetheless, it is worthwhile to note that our TesseraQ complies with standard uniform quantization formats and can be deployed with various kernels that support uniform quantization on various devices, e.g., GPU, CPU, TPU, edge processor.

Table 6: **Number (percentages) of rounding variables that flip after TesseraQ.**

| Bits/Layers | q_proj | k_proj | v_proj | o_proj | gate_proj | up_proj | down_proj |
|-------------|--------------|--------------|--------------|--------------|---------------|---------------|---------------|
| W4A16g128 | 498k (2.97%) | 477k (2.85%) | 520k (3.10%) | 620k (3.70%) | 1.77M (3.92%) | 1.81M (4.02%) | 1.91M (4.24%) |
| W2A16g128 | 765k (4.55%) | 734k (4.37%) | 758k (4.52%) | 961k (5.73%) | 3.00M (6.67%) | 2.99M (6.64%) | 3.21M (7.12%) |

Table 7: **Comparison of weight memory compression and inference throughput.** We measure LLaMA-3.1 series model under various bitwidth/backend. WM stands for weight memory, TP_n denotes inference throughput with a batch size of n (output token/s).

| LLaMA-3.1 | | 8B (1×A5000) | | | 70B (2×A100-80GB) | | | 405B (4×A100-80GB) | | |
|-----------|---------|--------------|--------|-----------|-------------------|--------|-----------|--------------------|--------|-----------|
| BitWidth | Backend | WM | TP_1 | TP_{16} | WM | TP_1 | TP_{16} | WM | TP_1 | TP_{16} |
| FP16 | Pytorch | 15GB | 49.23 | 358.1 | 132GB | 12.31 | 104.0 | 756GB | OOM | OOM |
| W4A16g128 | Exllama | 5.5GB | 57.54 | 361.1 | 39GB | 26.23 | 86.94 | 209GB | 7.01 | 18.59 |
| W2A16g128 | Triton | 3.9GB | 165.3 | 545.5 | 21GB | 4.93 | 54.35 | 114GB | 0.18 | 2.94 |

5 RELATED WORK

Quantization has been a primary method to compress and accelerate off-the-shelf large models. Survey papers by [Gholami et al. \(2022\)](#) and [Nagel et al. \(2021\)](#) have systematically summarized the progress of quantization. Here, we list several major quantization works, especially for LLMs.

Post-Training Quantization for LLMs. While Quantization aware Training (QAT) guarantees better task performance in low-bit quantization, PTQ is more suitable for LLM due to its less reliance on computing resources and training data. PTQ methods like [Frantar et al. \(2022\)](#); [Lin et al. \(2023\)](#); [Wei et al. \(2022; 2023\)](#); [Shao et al. \(2023\)](#); [Chee et al. \(2023\)](#); [Liu et al. \(2023a\)](#) improve the uniform quantization performance by optimizing weights, transformation scales, and clipping ranges. Our method continues improving the uniform quantization effect by incorporating rounding optimization. Other works try to improve PTQ in LLMs in different ways. For example, AQLM and GPTVQ ([Egiazarian et al., 2024](#); [van Baalen et al., 2024](#)) explore non-uniform quantization schemes for weight-only quantization, which may better match the distribution of weights. LLM.int8 ([Dettmers et al., 2022](#)), BiLLM ([Huang et al., 2024a](#)), SiLLM ([Huang et al., 2024b](#)) apply mixed-precision quantization to keep salient weights in high precision and maintain the accuracy. However, these methods cannot be applied to quantize activations and thus cannot support integer MatMul. QuaRot ([Ashkboos et al., 2024](#)), SpinQuant ([Liu et al., 2024](#)) target activation outliers and eliminate them through the rotation matrix. We have demonstrated that our method can also be combined with them.

QAT for LLM. Recent works also explore QAT-based quantization for LLMs. To reduce data access, LLM-QAT ([Liu et al., 2023b](#)) generates language data for data-free QAT. To prevent massive weight memory usage, Q-LoRA ([Dettmers et al., 2023](#)) applies quantization-aware low-rank adaptation for finetuning. Recently, BitNet and BitNet b.158 ([Wang et al., 2023](#); [Ma et al., 2024](#)) trained a 1-bit and 1.58-bit model from scratch, enabling multiplication-free LLM. However, these methods are hard to scale up due to the massive memory and computation requirements, especially for more than 70B models. As a result, they only focus on 1B~3B-scale models.

6 CONCLUSION

In this paper, we have proposed TesseraQ, a PTQ method for effectively calibrating large language models. Based on block reconstruction, TesseraQ optimizes weight rounding through a progressive approach that iteratively hardens and softens the rounding variables. Together with dequantization scale tuning, TesseraQ can be seamlessly combined with other PTQ methods like transformation, clipping, and rotation, to reach new state-of-the-art performance. We demonstrate TesseraQ’s superiority on open source LLaMA models. TesseraQ establishes a new state-of-the-art for quantized LLMs, in terms of perplexity, downstream accuracy and hardware performance.

Limitations. TesseraQ shares some limitations in terms of algorithm runtime, which may require longer processing time than existing baselines. For example, the LLaMA-2-7B takes 3~6 hours to finish the calibration process, while for AWQ/GPTQ, the calibration time is around 0.5 hours. Nevertheless, compared to QAT, our method still exhibits remarkable resource efficiency in required data and GPU memory. We leave how to accelerate rounding optimization in our future directions.

REFERENCES

- 540
541
542 Saleh Ashkboos, Amirkeivan Mohtashami, Maximilian L Croci, Bo Li, Martin Jaggi, Dan Alistarh,
543 Torsten Hoefler, and James Hensman. Quarot: Outlier-free 4-bit inference in rotated llms. *arXiv*
544 *preprint arXiv:2404.00456*, 2024.
- 545 Yonatan Bisk, Rowan Zellers, Jianfeng Gao, Yejin Choi, et al. Piqa: Reasoning about physical com-
546 monsense in natural language. In *Proceedings of the AAAI conference on artificial intelligence*,
547 volume 34, pp. 7432–7439, 2020.
- 548 Sébastien Bubeck, Varun Chandrasekaran, Ronen Eldan, Johannes Gehrke, Eric Horvitz, Ece Ka-
549 mar, Peter Lee, Yin Tat Lee, Yuanzhi Li, Scott Lundberg, et al. Sparks of artificial general
550 intelligence: Early experiments with gpt-4. *arXiv preprint arXiv:2303.12712*, 2023.
- 551 Jerry Chee, Yaohui Cai, Volodymyr Kuleshov, and Christopher De Sa. Quip: 2-bit quantization of
552 large language models with guarantees. *arXiv preprint arXiv:2307.13304*, 2023.
- 553 Wenhua Cheng, Weiwei Zhang, Haihao Shen, Yiyang Cai, Xin He, Kaokao Lv, and Yi Liu. Op-
554 timize weight rounding via signed gradient descent for the quantization of llms. *arXiv preprint*
555 *arXiv:2309.05516*, 2023.
- 556 Wei-Lin Chiang, Zhuohan Li, Zi Lin, Ying Sheng, Zhanghao Wu, Hao Zhang, Lianmin Zheng,
557 Siyuan Zhuang, Yonghao Zhuang, Joseph E. Gonzalez, Ion Stoica, and Eric P. Xing. Vicuna: An
558 open-source chatbot impressing gpt-4 with 90%* chatgpt quality, March 2023. URL <https://lmsys.org/blog/2023-03-30-vicuna/>.
- 559 Peter Clark, Isaac Cowhey, Oren Etzioni, Tushar Khot, Ashish Sabharwal, Carissa Schoenick, and
560 Oyvind Tafjord. Think you have solved question answering? try arc, the ai2 reasoning challenge.
561 *arXiv preprint arXiv:1803.05457*, 2018.
- 562 Tim Dettmers, Mike Lewis, Younes Belkada, and Luke Zettlemoyer. Llm.int8(): 8-bit matrix
563 multiplication for transformers at scale. *arXiv preprint arXiv:2208.07339*, 2022.
- 564 Tim Dettmers, Artidoro Pagnoni, Ari Holtzman, and Luke Zettlemoyer. Qlora: Efficient finetuning
565 of quantized llms. *arXiv preprint arXiv:2305.14314*, 2023.
- 566 Vage Egiазarian, Andrei Panferov, Denis Kuznedelev, Elias Frantar, Artem Babenko, and Dan Al-
567 istarh. Extreme compression of large language models via additive quantization. *arXiv preprint*
568 *arXiv:2401.06118*, 2024.
- 569 Elias Frantar, Saleh Ashkboos, Torsten Hoefler, and Dan Alistarh. Gptq: Accurate post-training
570 quantization for generative pre-trained transformers. *arXiv preprint arXiv:2210.17323*, 2022.
- 571 Amir Gholami, Sehoon Kim, Zhen Dong, Zhewei Yao, Michael W Mahoney, and Kurt Keutzer. A
572 survey of quantization methods for efficient neural network inference. In *Low-Power Computer*
573 *Vision*, pp. 291–326. Chapman and Hall/CRC, 2022.
- 574 Ruihao Gong, Yang Yong, Shiqiao Gu, Yushi Huang, Chentao Lv, Yunchen Zhang, Xianglong Liu,
575 and Dacheng Tao. Llmc: Benchmarking large language model quantization with a versatile com-
576 pression toolkit, 2024. URL <https://arxiv.org/abs/2405.06001>.
- 577 Wei Huang, Yangdong Liu, Haotong Qin, Ying Li, Shiming Zhang, Xianglong Liu, Michele Magno,
578 and Xiaojuan Qi. Billm: Pushing the limit of post-training quantization for llms. *arXiv preprint*
579 *arXiv:2402.04291*, 2024a.
- 580 Wei Huang, Haotong Qin, Yangdong Liu, Yawei Li, Xianglong Liu, Luca Benini, Michele Magno,
581 and Xiaojuan Qi. Slim-llm: Saliency-driven mixed-precision quantization for large language
582 models. *arXiv preprint arXiv:2405.14917*, 2024b.
- 583 Wei Huang, Xingyu Zheng, Xudong Ma, Haotong Qin, Chengtao Lv, Hong Chen, Jie Luo, Xiaojuan
584 Qi, Xianglong Liu, and Michele Magno. An empirical study of llama3 quantization: From llms
585 to mllms, 2024c. URL <https://arxiv.org/abs/2404.14047>.
- 586
587
588
589
590
591
592
593

- 594 Itay Hubara, Yury Nahshan, Yair Hanani, Ron Banner, and Daniel Soudry. Improving post
595 training neural quantization: Layer-wise calibration and integer programming. *arXiv preprint*
596 *arXiv:2006.10518*, 2020.
- 597
598 Albert Q Jiang, Alexandre Sablayrolles, Arthur Mensch, Chris Bamford, Devendra Singh Chaplot,
599 Diego de las Casas, Florian Bressand, Gianna Lengyel, Guillaume Lample, Lucile Saulnier, et al.
600 Mistral 7b. *arXiv preprint arXiv:2310.06825*, 2023.
- 601 JonathanSalwan. Jonathansalwan/triton: Triton is a dynamic binary analysis library. build your own
602 program analysis tools, automate your reverse engineering, perform software verification or just
603 emulate code. URL <https://github.com/jonathansalwan/Triton>.
- 604
605 Diederik P Kingma. Adam: A method for stochastic optimization. *arXiv preprint arXiv:1412.6980*,
606 2014.
- 607
608 Yuhang Li, Ruihao Gong, Xu Tan, Yang Yang, Peng Hu, Qi Zhang, Fengwei Yu, Wei Wang, and
609 Shi Gu. Brecq: Pushing the limit of post-training quantization by block reconstruction. *arXiv*
preprint arXiv:2102.05426, 2021.
- 610
611 Ji Lin, Jiaming Tang, Haotian Tang, Shang Yang, Xingyu Dang, and Song Han. Awq:
612 Activation-aware weight quantization for llm compression and acceleration. *arXiv preprint*
613 *arXiv:2306.00978*, 2023.
- 614
615 Jing Liu, Ruihao Gong, Xiuying Wei, Zhiwei Dong, Jianfei Cai, and Bohan Zhuang. Qllm:
616 Accurate and efficient low-bitwidth quantization for large language models. *arXiv preprint*
arXiv:2310.08041, 2023a.
- 617
618 Zechun Liu, Barlas Oguz, Changsheng Zhao, Ernie Chang, Pierre Stock, Yashar Mehdad, Yangyang
619 Shi, Raghuraman Krishnamoorthi, and Vikas Chandra. Llm-qat: Data-free quantization aware
620 training for large language models. *arXiv preprint arXiv:2305.17888*, 2023b.
- 621
622 Zechun Liu, Changsheng Zhao, Igor Fedorov, Bilge Soran, Dhruv Choudhary, Raghuraman Krish-
623 namoorthi, Vikas Chandra, Yuandong Tian, and Tijmen Blankevoort. Spinqant—llm quantization
624 with learned rotations. *arXiv preprint arXiv:2405.16406*, 2024.
- 625
626 Shuming Ma, Hongyu Wang, Lingxiao Ma, Lei Wang, Wenhui Wang, Shaohan Huang, Li Dong,
627 Ruiping Wang, Jilong Xue, and Furu Wei. The era of 1-bit llms: All large language models are in
628 1.58 bits. *arXiv preprint arXiv:2402.17764*, 2024.
- 629
630 Stephen Merity, Caiming Xiong, James Bradbury, and Richard Socher. Pointer sentinel mixture
631 models. *arXiv preprint arXiv:1609.07843*, 2016.
- 632
633 Meta. Introducing llama 3.1: Our most capable models to date, 2024. URL <https://ai.meta.com/blog/meta-llama-3-1/>.
- 634
635 Markus Nagel, Rana Ali Amjad, Mart Van Baalen, Christos Louizos, and Tijmen Blankevoort. Up or
636 down? adaptive rounding for post-training quantization. In *International Conference on Machine*
637 *Learning*, pp. 7197–7206. PMLR, 2020.
- 638
639 Markus Nagel, Marios Fournarakis, Rana Ali Amjad, Yelysei Bondarenko, Mart Van Baalen,
640 and Tijmen Blankevoort. A white paper on neural network quantization. *arXiv preprint*
arXiv:2106.08295, 2021.
- 641
642 Colin Raffel, Noam Shazeer, Adam Roberts, Katherine Lee, Sharan Narang, Michael Matena, Yanqi
643 Zhou, Wei Li, and Peter J Liu. Exploring the limits of transfer learning with a unified text-to-text
644 transformer. *The Journal of Machine Learning Research*, 21(1):5485–5551, 2020.
- 645
646 Keisuke Sakaguchi, Ronan Le Bras, Chandra Bhagavatula, and Yejin Choi. Winogrande: An adver-
647 sarial winograd schema challenge at scale. *Communications of the ACM*, 64(9):99–106, 2021.
- 648
649 Wenqi Shao, Mengzhao Chen, Zhaoyang Zhang, Peng Xu, Lirui Zhao, Zhiqian Li, Kaipeng Zhang,
650 Peng Gao, Yu Qiao, and Ping Luo. Omniquant: Omnidirectionally calibrated quantization for
651 large language models. *arXiv preprint arXiv:2308.13137*, 2023.

648 Hugo Touvron, Thibaut Lavril, Gautier Izacard, Xavier Martinet, Marie-Anne Lachaux, Timothée
649 Lacroix, Baptiste Rozière, Naman Goyal, Eric Hambro, Faisal Azhar, et al. Llama: Open and
650 efficient foundation language models. *arXiv preprint arXiv:2302.13971*, 2023a.
651

652 Hugo Touvron, Louis Martin, Kevin Stone, Peter Albert, Amjad Almahairi, Yasmine Babaei, Niko-
653 lay Bashlykov, Soumya Batra, Prajjwal Bhargava, Shruti Bhosale, et al. Llama 2: Open founda-
654 tion and fine-tuned chat models. *arXiv preprint arXiv:2307.09288*, 2023b.

655 Mart van Baalen, Andrey Kuzmin, Markus Nagel, Peter Couperus, Cedric Bastoul, Eric Mahurin,
656 Tijmen Blankevoort, and Paul Whatmough. Gptvq: The blessing of dimensionality for llm quan-
657 tization. *arXiv preprint arXiv:2402.15319*, 2024.

658 Hongyu Wang, Shuming Ma, Li Dong, Shaohan Huang, Huaijie Wang, Lingxiao Ma, Fan Yang,
659 Ruiping Wang, Yi Wu, and Furu Wei. Bitnet: Scaling 1-bit transformers for large language
660 models. *arXiv preprint arXiv:2310.11453*, 2023.

661

662 Xiuying Wei, Yunchen Zhang, Xiangguo Zhang, Ruihao Gong, Shanghang Zhang, Qi Zhang, Feng-
663 wei Yu, and Xianglong Liu. Outlier suppression: Pushing the limit of low-bit transformer lan-
664 guage models. *Advances in Neural Information Processing Systems*, 35:17402–17414, 2022.

665 Xiuying Wei, Yunchen Zhang, Yuhang Li, Xiangguo Zhang, Ruihao Gong, Jinyang Guo, and Xian-
666 glong Liu. Outlier suppression+: Accurate quantization of large language models by equivalent
667 and optimal shifting and scaling. *arXiv preprint arXiv:2304.09145*, 2023.

668

669 Rowan Zellers, Ari Holtzman, Yonatan Bisk, Ali Farhadi, and Yejin Choi. Hellaswag: Can a ma-
670 chine really finish your sentence? *arXiv preprint arXiv:1905.07830*, 2019.

671 Zixuan Zhou, Xuefei Ning, Ke Hong, Tianyu Fu, Jiaming Xu, Shiyao Li, Yuming Lou, Luning
672 Wang, Zhihang Yuan, Xiuhong Li, et al. A survey on efficient inference for large language
673 models. *arXiv preprint arXiv:2404.14294*, 2024.
674
675
676
677
678
679
680
681
682
683
684
685
686
687
688
689
690
691
692
693
694
695
696
697
698
699
700
701

A ABLATION STUDY ON ROUNDING OPTIMIZATION

In order to demonstrate the effectiveness of our proposed PAR, we compare our method with the several rounding optimization variants here.

AdaRound (Nagel et al., 2020). For AdaRound, the optimization is formulated by

$$\begin{aligned} \min_{\nu} \quad & \|\hat{\mathbf{W}}\mathbf{X} - \mathbf{W}\mathbf{X}\|_F^2 + \lambda \sum_{i,j} 1 - |2\sigma(\nu_{i,j}) - 1|^\beta, \\ \text{s.t.} \quad & \hat{\mathbf{W}} = \mathbf{s} \times (\mathbf{W}^q - \mathbf{z}), \quad \mathbf{W}^q = \text{clamp}\left(\left\lfloor \frac{\mathbf{W}}{\mathbf{s}} \right\rfloor + \sigma(\nu) + \mathbf{z}, 0, 2^N - 1\right). \end{aligned} \quad (10)$$

This method utilizes the layer-wise reconstruction objective and a regularization loss. Both λ and β control the strength of the regularization loss during optimization, which encourages the rounding variables to move towards 0 and 1.

AdaQuant (Hubara et al., 2020). This method directly utilizes the STE method to optimize the weights, given by

$$\begin{aligned} \min_{\nu} \quad & \|\hat{\mathbf{W}}\mathbf{X} - \mathbf{W}\mathbf{X}\|_F^2, \\ \text{s.t.} \quad & \hat{\mathbf{W}} = \mathbf{s} \times (\mathbf{W}^q - \mathbf{z}), \quad \mathbf{W}^q = \text{clamp}\left(\left\lfloor \frac{\mathbf{W} + \mathbf{V}}{\mathbf{s}} \right\rfloor + \mathbf{z}, 0, 2^N - 1\right), \quad \frac{\partial \lfloor x \rfloor}{\partial x} = 1. \end{aligned} \quad (11)$$

Note that AdaRound and AdaQuant have not implemented their method on LLMs before. Therefore, we implement their method on our own and use the default hyper-parameters in their paper. Specifically, we experiment with the LLaMA-2-7B W2A16g128 quantization case, where the model is uniformly initialized from the AWQ checkpoint. Each weight tensor will be optimized for 5000 iterations for a fair comparison. We compare 3 methods, AdaRound, AdaQuant, and our PAR, with either layer-wise objective (Eq. (2)) or block-wise objective (Eq. (3)). For AdaRound, we set the learning rate the same as our method and while for AdaQuant the learning rate was 1e-5. The results are shown in the Table below.

Generally, we find that PAR consistently outperforms the other two rounding methods regardless of which objective. We think the reason is that we explicitly control the hardness of rounding variables through the progressive approach. While AdaRound and AdaQuant, they are less optimized on LLMs and may require more hyper-parameter search.

Table 8: **Ablation study on rounding method.** The results are reported on LLaMA-2-7B W2A16g128 quantization.

| Rounding Method | Objective | WT2(↓) | C4(↓) |
|------------------|-----------|--------|-------|
| None (AWQ) | Layer | 14.65 | 18.67 |
| AdaRound | Layer | 10.68 | 15.67 |
| AdaQuant | Layer | 16.78 | 21.34 |
| PAR | Layer | 9.43 | 12.79 |
| None (OmniQuant) | Block | 11.06 | 16.34 |
| AdaRound | Block | 9.05 | 11.45 |
| AdaQuant | Block | 10.05 | 14.87 |
| PAR | Block | 6.82 | 10.77 |

B MORE EXPERIMENTAL RESULTS

In this section, we include additional experimental results from the main section.

B.1 RESULTS ON C4

We demonstrate the perplexity results on the C4 datasets in Table 9. Note that the OmniQuant results are re-evaluated using the official checkpoint, which is slightly higher than the original paper results (Shao et al., 2023). Since the evaluation protocol can be different across different papers,

we ensure use of the same evaluation protocol to compare different methods. Note, we restrict all models here from using the WikiText2 calibration data as the calibration data will affect the perplexity metric as shown in our ablation study. The improvements of our method over existing approaches are consistent with the results on the WikiText2 dataset.

Table 9: **Weight-only quantization results of LLaMA-1 and LLaMA-2 Models.** We report C4 perplexity in this table. *, † means initialized from AWQ, and OmniQuant, respectively.

| LLaMA1&2 / PPL↓ | | 1-7B | 1-13B | 1-30B | 1-65B | 2-7B | 2-13B | 2-70B |
|-----------------|------------------|--------------|--------------|--------------|-------------|--------------|--------------|-------------|
| FP16 | - | 7.08 | 6.61 | 5.98 | 5.62 | 6.97 | 6.46 | 5.52 |
| W2A16 | RTN | 1.3e5 | 5.6e4 | 2.7e4 | 2.2e4 | 4.8e4 | 7.2e4 | 2.4e4 |
| | GPTQ | 689.13 | 2.5e3 | 169.80 | 40.58 | NAN | 323.12 | 48.82 |
| | OmniQuant | 26.03 | 18.94 | 14.55 | 11.47 | 90.64 | 26.76 | 13.33 |
| | TesseraQ† | 13.28 | 11.43 | 10.81 | 8.52 | 14.82 | 11.96 | 9.15 |
| W2A16 g128 | RTN | 1.0e3 | 447.64 | 99.45 | 17.15 | 4.9e3 | 139.65 | 42.13 |
| | GPTQ | 27.71 | 15.29 | 11.93 | 11.99 | 33.70 | 20.97 | NAN |
| | AWQ | 16.35 | 12.93 | 10.07 | 8.78 | 18.67 | 11.88 | 8.49 |
| | OmniQuant | 14.06 | 11.27 | 10.37 | 8.65 | 16.34 | 12.14 | 9.33 |
| | TesseraQ* | 10.64 | 9.36 | 8.36 | 7.64 | 10.77 | 9.48 | 7.63 |
| W2A16 g64 | RTN | 151.43 | 76.00 | 30.07 | 11.34 | 475.35 | 28.69 | 13.43 |
| | GPTQ | 17.71 | 11.70 | 9.92 | 10.07 | 19.40 | 12.48 | NAN |
| | AWQ | 13.47 | 11.35 | 9.12 | 8.11 | 15.13 | 10.85 | 7.77 |
| | OmniQuant | 12.79 | 10.60 | 9.46 | 8.18 | 13.79 | 11.02 | 8.61 |
| | TesseraQ* | 10.32 | 9.05 | 8.18 | 7.48 | 10.50 | 9.23 | 7.44 |
| W3A16 | RTN | 28.26 | 13.22 | 28.66 | 12.79 | 402.35 | 12.51 | 10.02 |
| | GPTQ | 9.49 | 8.16 | 7.29 | 6.71 | 9.81 | 8.02 | 6.57 |
| | AWQ | 11.16 | 8.37 | 7.91 | 8.62 | 16.25 | 8.90 | 6.50 |
| | OmniQuant | 8.73 | 7.68 | 6.86 | 6.31 | 9.24 | 7.89 | 6.31 |
| | TesseraQ* | 8.15 | 7.38 | 6.60 | 6.16 | 8.30 | 7.41 | 6.08 |

Results on Smaller-Size LLM for Edge Inference. In addition to LLMs that are deployed on GPUs, we also test the performance of smaller-size LLMs geared for edge devices. We test LLaMA-3.2-1/3B models and compare them with AWQ in Table 10. We observe that our method significantly outperforms AWQ across different bitwidths in WikiText2 perplexity and average downstream task performance.

B.2 W4A8 QUANTIZATION

We also provide the W4A8 quantization in Table 11. Overall we find a small difference in W4A8 quantization due to the 8-bit per-token activation quantization.

B.3 DETAILED ACCURACY OF W4A4/W3A3 QUANTIZATION

Table 13 provides the detailed accuracy of each zero-shot tasks in W4A4/W3A3 quantization.

B.4 EVALUATION ON GENERALIZATION

To validate the generalization capability of our method, we test the quantization on LLaMA-2chat (Touvron et al., 2023b), an instruction-tuned model for chatbots. Following OmniQuant experiments (Shao et al., 2023), we use GPT-4 evaluation protocol (Chiang et al., 2023), performance is assessed on the Vicuna benchmark, which comprises 80 questions. We compare our TesseraQ and OmniQuant on LLaMA-2-7B-chat with W3A16g128 quantization. Our model has a 69% win rate against the OmniQuant model. We also demonstrate some chat cases in Fig. 4.

810
811
812
813
814
815
816
817
818
819
820
821
822
823
824
825
826
827
828
829
830
831
832
833
834
835
836
837
838
839
840
841
842
843
844
845
846
847
848
849
850
851
852
853
854
855
856
857
858
859
860
861
862
863

Table 10: Quantization Results of LLaMA-3.2 for edge inference.

| Bitwidths | Methods | LLaMA-3.2-1B | | LLaMA-3.2-3B | |
|-----------|------------------|--------------|--------------|--------------|--------------|
| | | WT2(↓) | Avg. (↑) | WT2(↓) | Avg. (↑) |
| FP16 | Pretrained | 9.75 | 56.50 | 7.81 | 63.57 |
| W2A16g128 | AWQ | 5475 | 35.42 | 495.2 | 38.15 |
| | TesseraQ* | 18.61 | 43.36 | 11.94 | 51.53 |
| W3A16g128 | AWQ | 16.69 | 49.85 | 10.21 | 59.94 |
| | TesseraQ* | 11.08 | 53.24 | 8.45 | 61.58 |
| W4A16g128 | AWQ | 10.85 | 54.68 | 8.25 | 62.83 |
| | TesseraQ* | 10.09 | 54.98 | 7.96 | 63.63 |

Table 11: Weight-activation quantization Results of various LLMs. We report the accuracy of 5 reasoning tasks (↑).

| Models | Bitwidths | Methods | PiQA | ArcE | ArcC | HellaSwag | WinoGrande | Avg. |
|--------------|-----------|------------------|--------------|--------------|--------------|--------------|--------------|--------------|
| LLaMA-7B | FP16 | - | 77.47 | 52.48 | 41.46 | 73.00 | 67.07 | 62.30 |
| | W4A8 | SmoothQuant | 75.19 | 70.45 | 37.45 | 51.06 | 64.87 | 59.81 |
| | | OS+ | 78.42 | 74.49 | 40.61 | 55.53 | 69.37 | 63.75 |
| | | TesseraQ* | 77.63 | 73.31 | 41.89 | 55.50 | 69.85 | 63.65 |
| LLaMA-2-7B | FP16 | - | 78.07 | 76.34 | 43.51 | 57.17 | 69.21 | 64.87 |
| | W4A8 | SmoothQuant | 75.24 | 70.95 | 38.39 | 51.30 | 63.85 | 59.95 |
| | | Outlier Supp.+ | 77.09 | 74.74 | 42.57 | 56.37 | 68.51 | 63.86 |
| | | TesseraQ* | 77.09 | 74.36 | 42.32 | 56.25 | 69.53 | 63.91 |
| LLaMA-3.1-8B | FP16 | - | 79.54 | 80.09 | 50.17 | 60.13 | 73.24 | 68.64 |
| | W4A8 | SmoothQuant | 71.98 | 66.37 | 34.55 | 50.46 | 67.40 | 58.16 |
| | | Outlier Supp.+ | 77.91 | 78.78 | 48.03 | 58.83 | 72.53 | 67.22 |
| | | TesseraQ* | 79.00 | 78.40 | 48.63 | 58.81 | 72.45 | 67.46 |
| Mistral-8B | W4A8 | SmoothQuant | 79.59 | 77.56 | 46.50 | 57.62 | 71.11 | 66.48 |
| | | OS+ | 80.35 | 79.04 | 48.03 | 60.18 | 72.45 | 68.02 |
| | | AWQ | 79.92 | 79.79 | 47.35 | 58.80 | 74.26 | 68.03 |
| | | TesseraQ* | 80.36 | 79.92 | 49.57 | 60.54 | 73.79 | 68.84 |

Table 12: Weight-activation quantization Results of Mistral-7B. We report the accuracy of 5 reasoning tasks (↑).

| Models | Bitwidths | Methods | PiQA | ArcE | ArcC | HellaSwag | WinoGrande | Avg. |
|------------------|-----------|------------------|--------------|--------------|--------------|--------------|--------------|--------------|
| Mistral-7B | FP16 | - | 80.68 | 80.93 | 50.42 | 61.26 | 73.79 | 69.42 |
| | W2A16g128 | GPTQ | 64.20 | 45.74 | 22.35 | 36.68 | 55.02 | 44.80 |
| | | AWQ | 68.44 | 56.73 | 27.44 | 40.60 | 56.03 | 49.06 |
| | | SignRound | 75.84 | 70.88 | 30.73 | 50.87 | 62.90 | 58.24 |
| | | TesseraQ* | 76.87 | 71.67 | 39.59 | 54.09 | 68.11 | 62.07 |
| | W3A16g128 | GPTQ | 79.70 | 78.70 | 48.41 | 59.15 | 71.98 | 67.19 |
| | | AWQ | 80.19 | 78.62 | 45.56 | 58.28 | 71.58 | 66.85 |
| | | SignRound | 79.54 | 78.70 | 46.33 | 59.60 | 72.85 | 67.40 |
| | | TesseraQ* | 79.59 | 78.36 | 47.44 | 59.87 | 71.98 | 67.45 |
| | W4A4 | SmoothQuant | 57.94 | 35.14 | 21.75 | 30.51 | 48.30 | 38.73 |
| OS+ | | 66.70 | 56.73 | 30.20 | 42.39 | 52.01 | 49.61 | |
| AWQ | | 66.26 | 54.16 | 30.80 | 43.45 | 53.67 | 49.67 | |
| TesseraQ* | | 72.19 | 65.90 | 33.78 | 49.02 | 57.61 | 55.71 | |

Table 13: **Detailed W4A4/W3A3 quantization results on each commonsense tasks of LLaMA-1/2/3.** We use per-channel weight quantization and per-token activation quantization *, † means initialized from AWQ, QuaRot.

| Models | Bitwidths | Methods | PiQA | ArcE | ArcC | HellaSwag | WinoGrande | Avg. | |
|------------------|------------------|------------------|-----------------|--------------|--------------|--------------|--------------|--------------|-------|
| LLaMA-7B | FP16 | - | 78.67 | 75.33 | 41.80 | 56.96 | 69.85 | 64.53 | |
| | | SmoothQuant | 55.49 | 31.22 | 21.16 | 27.31 | 49.88 | 37.02 | |
| | W4A4 | OS+ | 67.46 | 57.74 | 31.05 | 41.83 | 54.38 | 50.50 | |
| | | AWQ | 65.56 | 57.36 | 26.10 | 9.02 | 53.98 | 48.41 | |
| | | OmniQuant | 66.15 | 45.20 | 31.14 | 56.44 | 53.43 | 50.47 | |
| | | QLLM | 68.77 | 45.20 | 31.14 | 57.43 | 56.67 | 51.84 | |
| | | TesseraQ* | 71.98 | 64.77 | 32.67 | 47.59 | 60.22 | 55.45 | |
| | | Atom (W4A4g128) | 76.28 | 52.10 | 38.99 | 69.81 | 63.69 | 60.17 | |
| | | QuaRot | 71.70 | 64.81 | 30.88 | 48.25 | 61.24 | 55.38 | |
| | | GPTQ† | 76.55 | 72.60 | 37.11 | 53.67 | 66.93 | 61.37 | |
| | | TesseraQ† | 76.22 | 73.31 | 39.25 | 54.45 | 66.38 | 61.92 | |
| | | W3A3 | Atom (W3A3g128) | 65.56 | 41.41 | 30.72 | 53.19 | 55.56 | 49.28 |
| | QuaRot | | 52.72 | 26.09 | 20.82 | 26.06 | 51.93 | 35.53 | |
| | GPTQ† | | 68.98 | 58.92 | 26.87 | 43.90 | 55.40 | 50.82 | |
| TesseraQ† | 68.93 | | 57.78 | 27.30 | 43.24 | 58.24 | 51.10 | | |
| LLaMA-2-7B | FP16 | - | 78.07 | 76.34 | 43.51 | 57.17 | 69.21 | 64.87 | |
| | | SmoothQuant | 53.04 | 25.71 | 20.22 | 25.71 | 51.77 | 35.29 | |
| | W4A4 | OS+ | 66.86 | 56.52 | 29.60 | 41.93 | 56.19 | 50.23 | |
| | | AWQ | 64.80 | 53.87 | 30.20 | 43.11 | 57.93 | 49.99 | |
| | | OmniQuant | 65.94 | 43.94 | 30.80 | 53.53 | 55.09 | 49.86 | |
| | | QLLM | 67.68 | 44.40 | 30.89 | 58.45 | 56.59 | 51.60 | |
| | | TesseraQ* | 70.89 | 63.34 | 32.93 | 48.28 | 60.14 | 55.12 | |
| | | QuaRot | 66.54 | 55.51 | 25.76 | 37.80 | 52.25 | 47.57 | |
| | | GPTQ† | 75.89 | 71.96 | 39.85 | 54.12 | 65.43 | 61.45 | |
| | | TesseraQ* | 76.22 | 74.20 | 39.50 | 53.80 | 65.03 | 61.75 | |
| | | W3A3 | QuaRot | 51.74 | 25.54 | 22.86 | 25.84 | 49.88 | 35.18 |
| | | | GPTQ† | 64.31 | 47.21 | 22.18 | 36.08 | 53.27 | 44.62 |
| | TesseraQ† | | 68.28 | 56.82 | 28.58 | 41.96 | 55.01 | 50.13 | |
| | LLaMA-3.1-8B | FP16 | - | 79.54 | 80.09 | 50.17 | 60.13 | 73.24 | 68.64 |
| SmoothQuant | | | 54.24 | 27.90 | 19.79 | 26.87 | 51.61 | 36.09 | |
| W4A4 | | OS+ | 57.34 | 40.99 | 20.22 | 33.19 | 51.77 | 40.71 | |
| | | AWQ | 59.68 | 44.90 | 22.09 | 34.53 | 51.30 | 42.51 | |
| | | TesseraQ* | 67.08 | 59.09 | 27.13 | 43.88 | 57.14 | 50.87 | |
| | | QuaRot | 69.85 | 58.03 | 28.07 | 43.37 | 59.82 | 51.83 | |
| | | GPTQ† | 76.22 | 73.94 | 41.21 | 55.47 | 67.48 | 62.87 | |
| | | TesseraQ† | 77.64 | 77.27 | 44.80 | 56.03 | 69.85 | 65.12 | |
| | | W3A3 | QuaRot | 52.28 | 26.59 | 20.56 | 26.11 | 50.67 | 35.25 |
| | | | GPTQ† | 56.96 | 33.62 | 20.47 | 28.87 | 49.40 | 37.87 |
| TesseraQ† | | 66.05 | 51.59 | 24.40 | 40.59 | 53.98 | 47.33 | | |
| LLaMA-3.1-70B | | FP16 | - | 83.13 | 87.12 | 60.92 | 66.47 | 79.56 | 75.44 |
| | | | SmoothQuant | 57.45 | 38.46 | 24.23 | 30.22 | 54.93 | 41.06 |
| | | W4A4 | OS+ | 53.04 | 25.79 | 22.01 | 25.88 | 48.85 | 35.12 |
| | AWQ | | 69.91 | 61.71 | 34.04 | 47.98 | 54.61 | 53.65 | |
| | TesseraQ* | | 78.29 | 69.15 | 38.12 | 53.74 | 61.16 | 60.09 | |
| | QuaRot | | 57.88 | 36.36 | 19.02 | 28.13 | 53.19 | 38.92 | |
| | GPTQ† | | 79.76 | 80.17 | 50.59 | 60.71 | 73.08 | 68.87 | |
| | TesseraQ† | | 81.84 | 82.64 | 54.07 | 63.90 | 65.64 | 69.62 | |
| | W3A3 | | QuaRot | 52.06 | 24.87 | 20.05 | 25.55 | 49.25 | 34.26 |
| | | | GPTQ† | 55.98 | 34.80 | 19.45 | 28.38 | 51.46 | 38.02 |
| TesseraQ† | 74.80 | 66.03 | 36.42 | 51.34 | 58.43 | 57.42 | | | |

918
919
920
921
922
923
924
925
926
927
928
929
930
931
932
933
934
935
936
937
938
939
940
941
942
943
944
945
946
947
948
949
950
951
952
953
954
955
956
957
958
959
960
961
962
963
964
965
966
967
968
969
970
971



Figure 4: Examples of chat cases on Vicuna Benchmark (Chiang et al., 2023). We compare TesseraQ W3A16g128 and OmniQuan W3A16g128 quantization on LLaMA-2-7B-chat.